51st AIAA Aerospace Sciences Meeting including the New Horizons Forum and Aerospace Exposition
07 - 10 January 2013, Grapevine (Dallas/Ft. Worth Region), Texas

AIAA 2013-0265

Predictive Inner-Outer Model for Turbulent Boundary Layers Applied to Hypersonic DNS Data

Clara Helm* and M. Pino Martin †

The inner-outer predictive wall model of Mathis et al.[1] is applied to direct numerical simulation (DNS) data of supersonic and hypersonic turbulent boundaries with Mach 3 and Mach 7 freestream conditions. The model is based on an amplitude modulation of the energized structures in the inner layer by large scale momentum fluctuations in the logarithmic layer. Evidence that this modulating effect exists in the supersonic case is provided. Two sets of universal inner layer signals are calibrated from each of the DNS data sets. The model is extended to include near-wall predictions of temperature and density fluctuations. To test the model, inner layer predicted signals are built using filtered outer velocity signals from the DNS data sets as input to the model. Statistics of the predicted variables are compared to those of the original DNS data.

I. Introduction

Many articles have been written on the existence and organization of coherent structures in wall bounded turbulent flows. The idea of a hairpin, or horseshoe, vortex was first introduced in 1952 by Theodorsen.[2] Adrian, Meinhart and Tomkins[3] and also Ganapathisubramani, Longmire, and Marusic[4] observed that these hairpin vortices align themselves into very long regions of 'packet' groupings that can extend as much as 20δ in the streamwise direction thus earning the name 'superstructures' as coined by Hutchins and Marusic.[5] These structures are known to induce low momentum streaks beneath them which are felt through the inner layer down to the wall surface.[6]

The majority of the past research on near-wall structures in turbulent boundary layers has been done using incompressible data.[3,5–11] A few studies have been done on the structure of compressible turbulent boundary layers and in general the same structural behavior is observed. The series of papers by Lian, Beekman, and Martin[12–14] on DNS of hypersonic turbulent boundary layers demonstrates the existence of large scale coherent structures in boundary layers of freestream Mach numbers ranging from 0 to 12 by using two-point correlations of the streamwise momentum fluctuations. In the same series of papers Duan et al. also provided contour plots of momentum fluctuations in the near-wall region where long, low momentum streaks similar to the results from incompressible data could be seen. Other works on the structure of compressible turbulent boundary layers are by Riguette, Wu, and Martin[15] who investigated structures in a Mach 3 boundary layer, O'Farrel and Martin[16] who developed a method of tracking hairpin packets in Mach 3 DNS data, and Beekman, Priebe, and Martin[17] who performed spectral analysis on DNS data of a Mach 3 spatially developing turbulent boundary layer.

There is reason to believe that the large-scale coherent structures that reside in the logarithmic layer have an effect on the near-wall turbulence cycle. It was proposed by Mathis, Hutchins, and Marusic[18] that the large-scale momentum fluctuations caused by superstructures in the logarithmic layer modulate the energized, small-scale fluctuations in the viscous sublayer. The same authors later developed a predictive model for the streamwise velocity fluctuations in the inner-layer based on this modulating effect.[1] They were able to show that a statistically accurate inner velocity signal can be constructed using only what they refer to as a 'universal' signal that is independent of Reynolds number effects and a signal of the large-scale component of the streamwise velocity taken from a point roughly in the middle of the logarithmic layer. This model is especially appealing for use as a wall boundary condition in a large eddy simulation (LES) since, assuming the universal signal is known, a filtered velocity signal from the logarithmic layer would be

*Graduate Student, Department of Aerospace Engineering, Universigy of Maryland, College Park.
†Associate Professor, Department of Aerospace Engineering, University of Maryland, College Park.

Case	δ (m)	U_∞ (m/s)	u_τ (m/s)	z_τ (m)	Re_τ
M3	0.013	610.5	29.7	1.85e-5	640
M7	0.036	1147.8	64.3	6.50e-5	559

Table 1. Flow variables for Mach 3 and Mach 7 taken at the computational domain recycling stations

all that is needed to produce a statistically accurate inner signal. In this paper the wall model of Mathis et al.[1] is applied to supersonic and hypersonic turbulent boundary layer data where the correct scalings to account for compressibiltiy[12–14] are included in the model.

The wall model is applied to two DNS data sets of turbulent boundary layers with free stream Mach numbers of 3 and 7. In Section II the two flow fields and a short description of the computational methods are presented. In Section III evidence of the small scale modulating effect in the compressible DNS data are shown. In Section IV the universal signals are obtained from the DNS and in Section V predicted signals are constructed and compared statistically to the original DNS data. Lastly, conclusions are given in Section IV.

II. Computational Setup and Flow Details

The data sets are two direct numerical simulations of spatially developing, zero pressure gradient turbulent boundary layers with adiabatic wall-temperature conditions. The two flows are at freestream Mach numbers of 2.9 and 7.2 referred to throughout this paper as the Mach 3 and Mach 7 cases. The simulations were initialized using the method outlined by Martin.[19] The boundary conditions at the inflow were prescribed using the recycling-rescaling method of Xu and Martin.[20] Supersonic exit boundary conditions were applied to the top and outlet of the domain. Periodic boundary conditions were prescribed in the spanwise direction. A bandwidth optimized, weighted essentially non-oscillatory or WENO method was used for the computation of the inviscid fluxes[21] while the viscous fluxes were computed using a 4th-order accurate central differencing scheme. A 3rd-order, explicit Runge-Kutta scheme was used for time integration.

In order to prevent any forcing by large, coherent eddies in the rescaling method, very long computational domains were used for both simulations with streamwise lengths on the order of 60 boundary layer thicknesses. The domain sizes are approximately $(60 \times 10 \times 10)\delta_0$ for the Mach 3 flow and $(55 \times 10 \times 20)\delta_0$ for the Mach 7 flow where δ_0 is the boundary layer thickness at the inlet. High frequency time signals are output at the recycling plane located near the outlet of the computational domains. The time signals span a total time length of $400\delta/U_\infty$ and $200\delta/U_\infty$ for the Mach 3 and Mach 7 flows respectively. The sample rate of the signals are on the order of $100U_\infty/\delta$ for both signals. Because the analysis presented in this paper is done using these time signals, a list of important flow conditions evaluated at the recycling plane are listed in table 1. In the table, δ is the local boundary layer thickness and U_∞ is the freestream velocity. The friction velocity u_τ is defined as $u_\tau = \sqrt{\rho_w/\tau_w}$ and the viscous length scale is defined as $z_\tau = \nu_w/u_\tau$ where ν_w is the dynamic viscosity at the wall. The Reynolds number is $Re_\tau = \delta/z_\tau$.

III. Amplitude Modulation

Before the wall model can be applied to the supersonic boundary layers, it is necessary to demonstrate that the physics behind the model, that is the modulating effect, occurs in compressible conditions and on the DNS data. Mathis et al.[18] showed that the energized, small-scale motions in the inner layer of wall-bounded flows are subject to a modulating effect by the large-scale fluctuations in the logarithmic layer. That is, positive, large-scale momentum fluctuations in the logarithmic layer intensify the inner layer small-scale fluctuations beneath them and negative, large-scale momentum fluctuations suppress these small-scale fluctuations. Mathis et al.[18] were able to quantify this observation by using a Hilbert transform to acquire a time signal representative of the envelope of the inner, small-scale fluctuations and then correlating it with a time signal of the outer, large-scale fluctuations. In addition, Mathis et al.[18] have shown that the modulating effect diminishes with Reynolds number and, since the Reynolds number of the data they used to demonstrate the modulating effect is significantly greater than in the current DNS data sets ($Re_\tau = 7300$ compared to our $Re_\tau \approx 600$), it seems obligatory to verify that the Reynolds number in the current simulations is not too

Case	Filter Order	Duration	Cutoff λ	Cutoff Freq.
	samples	δ/U_e	z_τ	U_e/δ
M3	2600	22.9	7000	0.084
M7	3600	24.3	7000	0.068

Table 2. Parameters for Finite Impulse Response Filter

low for application of the model.

A brief outline of the method of velocity signal decomposition and modulation analysis as presented in the paper by Mathis et al.[18] is given here. Consider a single time signal of streamwise velocity fluctuations u' normalized by friction velocity u_τ. Here u' represents a fluctuation about the Reynolds averaged quantity $\bar{u}$' A low-pass filter is used to separate the signal into a large-scale component u_L^+ and a small-scale component u_S^+. No further modifications are made to the large-scale component, however, a Hilbert transform (referred to here as $E()$) is applied to the small-scale signal. The Hilbert transform provides an envelope of the small-scale fluctuations. The envelope $E(u_S^+)$ is next low-pass filtered using the same filter as was used to extract u_L^+ so that a modulation of the same order of scales as u_L^+ can be considered. The two time signals u_L^+ and $E_L(u_S^+)$ are correlated to get the amplitude modulation coefficient referred to throughout this paper as R and is defined by equation 1.

$$R = \frac{\overline{u_L^+ E(u_s^+)}}{\sqrt{\overline{u_L^{+2}}}\sqrt{\overline{E(u_s^+)^2}}} \tag{1}$$

Before it is possible to apply equation 1 to our DNS data, a low-pass filter must be defined for the large/small-scale decomposition. A cutoff wavelength for the filter must be chosen so that all scales bellow the cutoff are representative of the energized small scales and all scales above the cutoff are representative of the superstructure signals. Mathis et al.[18] used a cutoff normalized by z_τ of $\lambda^+ = 7000$ which, if plotted over the pre-multiplied power spectra $k_x\phi_{uu}$ of the Mach 3 and Mach 7 data as shown in figures 1 (a) and (b), seems to be a reasonable cutoff for our data as well. As can be seen in figures 1 (a) and (b), the inner layer peak in the spectra is well within the cutoff. Once the cutoff wavelength is determined, the low-pass filter can be defined. In this analysis a finite impulse response (FIR) filter is used. The parameters of this filter are provided in table 2.

To quantify the amount of global amplitude modulation in the inner layer, R is calculated for a range of wall-normal locations, z^+. When calculating R, the large-scale signal is always taken at $z^+ = 100$ and the small-scale amplitude envelope is taken at the local z^+. The location $z^+ = 100$ coincides roughly with the center of the logarithmic layer as can be seen in the van Driest transformed velocity profiles plotted in figure 2. The resulting correlation curves are shown plotted versus wall-normal distance in figure 3. For both Mach number cases large values of R are seen throughout the inner region of the boundary layer below $z^+ \approx 10$. The correlation curves decrease rapidly and cross the zero point at $z^+ \approx 20$ and become negative in the logarithmic layer and the wake. This trend is very similar to that seen by Mathis et al.,[18] however, in their data the zero crossing of the curve occurs closer to the center of their logarithmic layer and there is a slight plateau between this point and the inner peak in R. This difference may be attributed to the existence of a second energy peak in their data located at larger frequencies in the logarithmic layer. This outer peak forms at higher Reynolds number conditions.[18] At any rate, the correlation provides evidence that the near-wall, small-scale turbulence is being modulated by the large fluctuations in the logarithmic layer in the DNS data.

IV. The Universal Signals

Two sets of universal signals are calibrated from the DNS data time signals that are output at the rescaling planes near the domain ends. The purpose of producing two sets of universal signals is to demonstrate through comparison of the two signals that the method outlined below properly removes any effects of compressibility. The reader is referred to the paper of Mathis et al.[1] for details of the calibration process, but in short the universal signal is obtained by taking known data from either a simulation or experiment and removing the Reynolds number effect by simply removing the modulating effect and any linear superposition of the outer

signal onto the inner layer.

The model equation proposed by Mathis et al.[1] is repeated here in equation 2.

$$u_p^+(z^+) = u^*(z^+)1 + \beta u_{OL}^+(z_O^+, \theta_L) + \alpha u_{OL}^+(z_O^+, \theta_L) \tag{2}$$

Here u_P^+ is the predicted signal of streamwise fluctuations and u^* is the universal signal. Both the predicted and universal signals are functions of the wall-normal location z^+. As mentioned, equation 2 shows that the inner predicted signal is a combination of (i) the modulation of the universal signal by the large-scale motions in the logarithmic layer (first term on the right hand side) and (ii) the linear superposition of the large scale motions onto the universal signal (second term on the right hand side). The large-scale signal in the logarithmic layer is indicated by u_{OL}^+ in equation 2. The wall-normal distance z_O^+ is the location at which u_{OL}^+ is taken and corresponds to a point roughly in the middle of the logarithmic layer. The parameters α, β, and θ_L are referred to as the 'universal parameters'. The α is the coefficient for linear superposition of the outer signal onto the inner signal and β is the modulation coefficient. The angle θ_L represents a shifting of u_{OL}^+ in time and is related to the inclination angle of the superstructures.

Mathis et al.[1] use experimental subsonic hotwire probe data in a calibration experiment to determine values for the universal parameters and u^*. The same calibration procedure is carried out for both our DNS data sets to obtain two sets of uinversal parameters and two universal inner signals. To do this, u_P^+ and u_{OL}^+ in equation 2 are taken from the DNS raw time signals output from the rescaling station of the domain. The equation $z_O^+ = 3.9Re_\tau^{1/2}$ suggested by Mathis et al.[1] is used to determine the location of the outer signal resulting in $z_O^+ = 102.4$ and 92.3 for the Mach 3 and Mach 7 cases respectively. Also, a convection velocity of the large scale structures in the logarithmic layer has to be assumed in order to determine θ_L. As is suggested by Mathis et al,[1] the mean velocity at the outer point z_O^+ is taken to be the superstructure convection velocity. The resulting parameters for both data sets are shown in figures 4 (a), (b), and (c). In figure 4 (a) the two solutions for α differ only slightly. The lean angle θ_L plotted in figure 4 (b) show nearly the same trend but the Mach 7 solution results in higher angles. This is consistent with the findings of Duan, Beekman, and Martin[13] that the inclination angle of the superstructures appears to increase for higher Mach number flows. The superposition coefficient β plotted in figure 4 show similar trends between the Mach 3 and Mach 7 solutions and both curves show an identical trend to the curves of the modulation coefficient in figure 3.

Since the data are compressible the effect of density scaling must also be removed (in addition to the modulation and superposition) from the raw signals in order to obtain truly be universal signals. Duan, Beekman, and Martin[12–14] showed that the streamwise turbulence intensities profiles u'_{rms}/u_τ collapse quite well when the density scaling of Morkovin's hypothesis is applied. This was demonstrated with turbulent boundary layers of freestream Mach numbers ranging from M0 to M12. The universal signal must then be divided by the density scaling $(\sqrt{\bar{\rho}(z^+)}/\sqrt{\rho_w})$ where $\bar{\rho}$ and ρ_w are from the data set used for calibrating u^*. As a result, $u^*(z^+)$ in equation 2 must be replaced with $(\sqrt{\rho_w}/\sqrt{\bar{\rho}(z^+)})u^*$ where ρ_w and $\bar{\rho}$ are profiles of the flow conditions being modeled. In figure 5, (a) the streamwise turbulence intensity profiles for the universal signals are plotted before scaling and in figure 5 (b) after scaling. There is better agreement in the profile shape and the wall-normal location of the maximum value in the density weighted profiles.

V. The Predicted Signals and Statistical Evaluation

The model of equation 2 is next tested using the universal signals and parameters to create predicted inner layer signals at the same flow conditions as the original DNS simulations. A predicted signal of the Mach 3 boundary layer is made using first the universal signals and parameters calibrated from the Mach 3 flow and then again using the universal signal and parameters calibrated from the Mach 7 flow. The same is done for predictions of the Mach 7 inner layer. This process is explained below.

First, by assuming Taylor's Hypothesis, the universal signals are converted from time signals to a spatial volume by using the mean velocity profile of the flow conditions being modeled. The size of the volume for the predicted signals is chosen to be 10δ in the streamwise direction and the same size as the original DNS domain in the spanwise direction. The wall-normal extent of the volumes is limited by the location of z_O^+ as defined in Section III. The input to the model u_{OL}^+ is taken from a single timestep spatial volume of the DNS data set of the conditions being modeled. The $u_{OL}^+ is$ then filtered using the same filter as described in Section III. Before being input into the model, the spatial outer signal has to be trimmed from the streamwise length of the DNS domain to the same length as the predicted signal domain. The outer signal is trimmed

so that the desired 10δ long section is taken as a section centered about the recycling plane of the original DNS. The purpose of this is to produce predicted signals with the same flow conditions as at the recycling planes of the DNS.

To converge the statistics of the predicted flowfields multiple volumes are computed and the statistics are averaged over the volumes. The outer signals for the series of volumes are taken from DNS volumes separated in time by a flow-through time that is based on the superstructure convection velocity and the streamwise extent of the predicted signal domain. That is, the outer signal is taken from single timestep volumes of the DNS that are separated in time by $\Delta t = 10\delta * U_c$ where the convection velocity U_c is the mean velocity at z_O^+. For both Mach number conditions only six volumes are needed to converge the statistics. In figures 6 (a) and 6 (b) are shown the profiles of the density weighted streamwise velocity intensities of the predicted Mach 3 and Mach 7 flows respectively. The statistics of the modeled flows match the DNS profile quite well and in both figures very little difference is seen between the prediction from the u^* calibrated from the Mach 3 data and the prediction from the u^* calibrated from the Mach 7 data. This suggests that the density scaling of the universal signal is sufficient in removing the compressibility effects from the universal signal.

An inner signal of temperature fluctuations can be constructed from the predicted velocity fields by using the Strong Reynolds Analogies (SRA)s. Morkovin proposed five SRAs two of which are equations 3 and 4.[22]

$$\frac{T'_{RMS}/\bar{T}}{(\gamma-1)M_a^2(u'_{RMS}/\bar{u})} \approx 1 \tag{3}$$

$$R_{u'T'} \approx -1 \tag{4}$$

Here 'RMS' stands for 'root-mean-squared', γ is the ratio of specific heats taken to be 1.4, and M_a is the local Mach number. A predicted inner temperature signal can be modeled by replacing u'_{RMS} and T'_{RMS} in equation 3 with the fluctuations u' and T' and the fluctuation direction from the relation in equation 4 which states that the velocity and time fluctuation signals are perfectly anticorrelated. The validity of a number of different versions of the SRAs of equation 3 and equation 4 were evaluated for compressible turbulent boundary layer at different conditions of Mach number, wall temperature, and enthalpy levels in the series of papers by Duan, Beekman, and Martin.[12–14] The equations in the form presented here were found to be reasonably accurate for the current Mach number and wall temperature conditions. In figures 7 (a) and 7 (b) are the predicted $T'_{RMS}/\bar{T}$ profiles for the Mach 3 and Mach 7 flow conditions respectively. All four predicted curves show good agreement with the DNS data.

In addition to temperature signals, the inner density fluctuations can be estimated from the modeled temperature fluctuations if the variations in pressure throughout the inner layer are assumed to be negligible. The relation of equation 5 follows from the ideal gas law.

$$\frac{\rho'}{\bar{\rho}} \approx -\frac{T'}{\bar{T}} \tag{5}$$

The RMS profiles of the density fluctuations modeled by equation 5 are plotted with the DNS data profile for Mach 3 in figure 8 (a) and Mach 7 in figure 8 (b). The density agrees fairly well for the Mach 3 but underestimates significantly the density fluctuations of the Mach 7 flow.

As a correction to the relation of equation 5, it is proposed that the ratio of density fluctuations over temperature fluctuations increases approximately linearly with Mach number. Therefore a scaling function $f(M)$ is introduced into equation 5 and the following new model equation is suggested.

$$\frac{\rho'}{\bar{\rho}} \approx -f(M)\frac{T'}{\bar{T}} \tag{6}$$

The supersonic turbulent boundary layer data of Duan, Beekman, and Martin[13] is used to determine the function $f(M)$ empirically. This data ranges in freestream Mach numbers between 3 and 12. A line is fit to data points of $(\rho'_{RMS}/\bar{\rho})/(T'_{RMS}/\bar{T})$ plotted against Mach number and the result is shown in figure 9. The error in the line fit ranges from approximately 5% at Mach 3 to 10% at Mach 12. The curve is also very nearly 1 at $M = 0$ as would be expected for incompressible flow. This new density scaling is next applied to the predictions of $\rho'_{RMS}/\bar{\rho}$ with a factor of 1.13 for the Mach 3 case and a factor of 1.25 for the Mach 7. As is seen in figures 10 (a) and (b) for Mach numbers 3 and 7 respectively, a much more accurate prediction is obtained.

VI. Conclusions

Using data from two direct numerical simulations of Mach 3 and Mach 7 turbulent boundary layers, two sets of universal signals and parameters were calibrated. In keeping with the term 'universal' very little difference was seen between the resulting superposition coefficients α and very similar trends were observed between the structure lean angle θ_L and the superposition coefficient β. The universal signals corrected for the Morkovin density scaling were also found to compare quite well when profiles of streamwise fluctuation intensities were compared. Ideally one could obtain just one set of the universal inner velocity signal and the corresponding parameters and be able to construct predicted inner signals for a range of flow conditions such as for different Reynolds numbers or Mach numbers for example. The successful reproduction of the statistics of the streamwise fluctuation intensities by using either set of universal signal and parameters as shown in Section IV seems to provide further confirmation that this is the case. In addition to the predicted streamwise velocity signals, temperature and density fluctuations were also predicted by using the strong Reynolds analogies and the equation of state. The Temperature statistics compared well with the DNS however, for the Mach 7 case, the density is not so well matched. To correct this a scaling of the density fluctuations with Mach number was introduced resulting in more accurate predictions.

Acknowledgments

This work is supported by the Air Force Office of Scientific Research under grant AF/9550- 10-1-0535 STW 21 - Revitalization of the Hypersonics Testing and Evaluation Workforce.

References

[1]Mathis, R., Hutchins, N., and Marusic, I., "A predictive inner-outer model for streamwise turbulence statistics in wall-bounded flows," *Journal of Fluid Mechanics*, Vol. 681, 2011, pp. 537–566.

[2]Theodorsen, T., "Mechanism of Turbulence," *2nd Proc. Midwestern Conference on Fluid Mechanics*, 1952.

[3]Adrian, R., Meinhart, C., and Tomkins, C., "Vortex organization in the outer region of the turbulent boundary layer," *Journal of Fluid Mechanics*, Vol. 422, 2000, pp. 1–54.

[4]Ganapathisubramani, B., Longmire, E. K., and Marusic, I., "Characteristics of vortex packets in turbulent boundary layers," *Journal of Fluid Mechanics*, Vol. 478, 2003, pp. 35–46.

[5]Hutchins, N. and Marusic, I., "Evidence of very long meandering features in the logarithmic region of turbulent boundary layers," *Journal of Fluid Mechanics*, Vol. 579, 2007, pp. 1–28.

[6]Kim, K. C. and Adrian, R. J., "Very large-scale motion in the outer layer," *Physics of Fluids*, Vol. 11, No. 2, 1999, pp. 417–422.

[7]Head, M. and Bandyopadhyay, P., "New aspects of turbulent boundary layer structure," *Journal of Fluid Mechanics*, Vol. 107, 1981, pp. 297–338.

[8]Balakumar, B. J. and Adrian, R. J., "Large- and very-large-scale motions in turbulent pipe flow," *Phil. Trans. R. Soc. A*, 2007.

[9]Guala, M., Hommema, S. E., and Adrian, R. J., "Large-scale and very-large-scale motions in turbulent pipe flow," *Journal of Fluid Mechanics*, Vol. 554, 2006, pp. 521–542.

[10]Hutchins, N. and Marusic, I., "Large-scale influences in near-wall turbulence," *Phil. Trans. R. Soc. A*, Vol. 365, 2007, pp. 647–664.

[11]Tomkins, C. and Adrian, R. J., "Spanwise structure and scale growth in turbulent boundary layers," *Journal of Fluid Mechanics*, Vol. 490, 2003, pp. 37–74.

[12]Duan, L. and Martin, M. P., "Direct numerical simulation of hypersonic turbulent boundary layers. Part II: Effect of wall temperatu re," *Journal of Fluid Mechanics*, Vol. 655, 2010, pp. 419–445.

[13]Duan, L., Beekman, I., and Martin, M. P., "Direct numerical simulation of hypersonic turbulent boundary layers. Part III: Effect of Mach number," *Journal of Fluid Mechanics*, Vol. 672, 2010, pp. 245–267.

[14]Duan, L., Beekman, I., and Martin, M. P., "Direct numerical simulation of hypersonic turbulent boundary layers. Part 4: Effect of high enthalpy," *Journal of Fluid Mechanics*, 2011, pp. 25–59.

[15]Ringuette, M. J., Wu, M., and Martin, M. P., "Coherent structures in direct numerical simulation of turbulent boundary layers at Mach 3," *Journal of Fluid Mechanics*, Vol. 594, 2008, pp. 59–69.

[16]O'Farrel, C. and Martin, M. P., "Chasing eddies and their wall signature in DNS of turbulent boundary layers," *Journal of Turbulence*, Vol. 10, No. 15, 2009, pp. 1–22.

[17]Beekman, I., Priebe, S., Kan, Y., and Martin, M. P., "DNS of a Large-Domain, Mach 3 Turbulent Boundary Layer: Turbulence Structure," *AIAA Paper No. 2011-755*, Jan. 2011.

[18]Mathis, R., Hutchins, N., and Marusic, I., "Large-scale amplitude modulation of the small-scale structures in turbulent boundary layers," *Journal of Fluid Mechanics*, Vol. 628, 2009, pp. 311–337.

[19]Martin, M. P., "Direct numerical simulation of hypersonic turbulent boundary layers. Part1: Initialization and comparison with experiments," *Journal of Fluid Mechanics*, Vol. 570, 2007, pp. 347–364.

[20]Xu, S. and Martin, M., "Assessment of Inflow Boundary Conditions for Compressible Turbulent Boundary Layers," *Physics of Fluids*, Vol. 16, 2004, pp. 2623–2639.

[21]Martin, M. P., Taylor, E. M., Wu, M., and Weirs, V. G., "A Bandwidth-Optimized WENO Scheme for the Direct Numerical Simulation of Compressible Turbulence," *Journal of Compressible Physics*, Vol. 220, 2006, pp. 270–289.

[22]Morkovin, M. V., "Effects of compressibility on turbulent flows," *In Mecanique de la Turbulence NRS*, 1962.

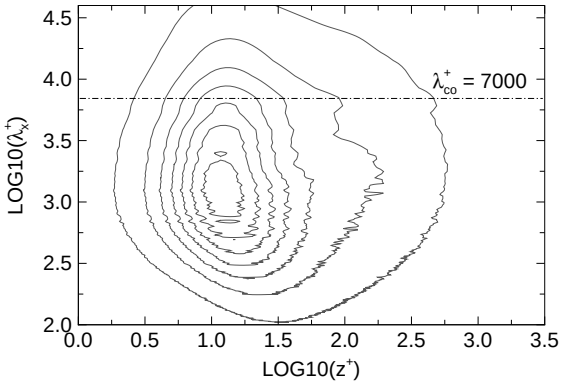

(a)

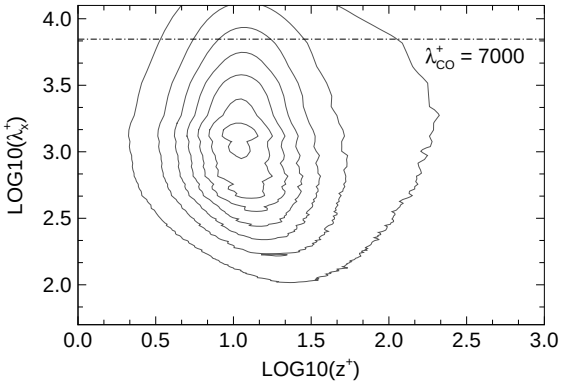

(b)

Figure 1. Premultiplied power spectrum of streamwise velocity fluctuations $k_x \phi_u u$ for (a) Mach 3 and (b) Mach 7.

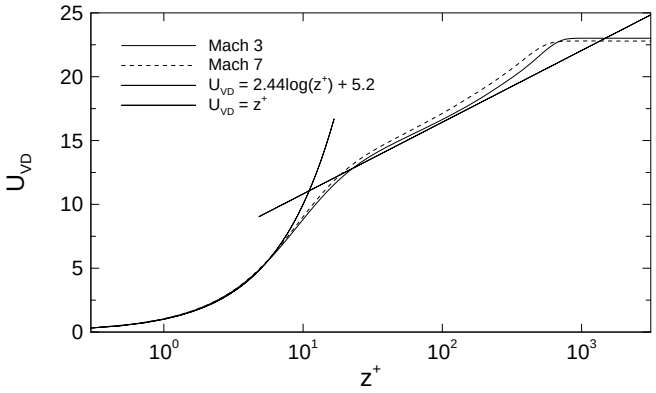

Figure 2. Van Driest transformed velocity profiles for Mach 3 and Mach 7.

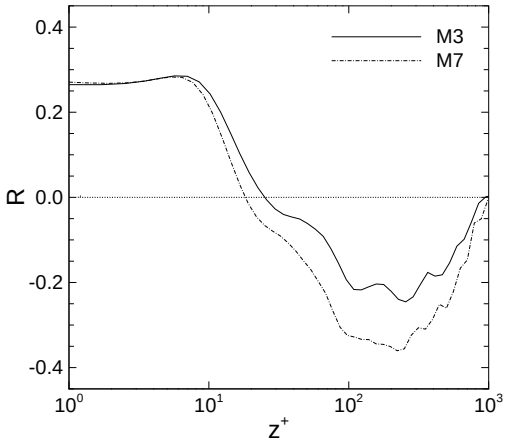

Figure 3. Modulation correlation versus wall-normal distance z^+.

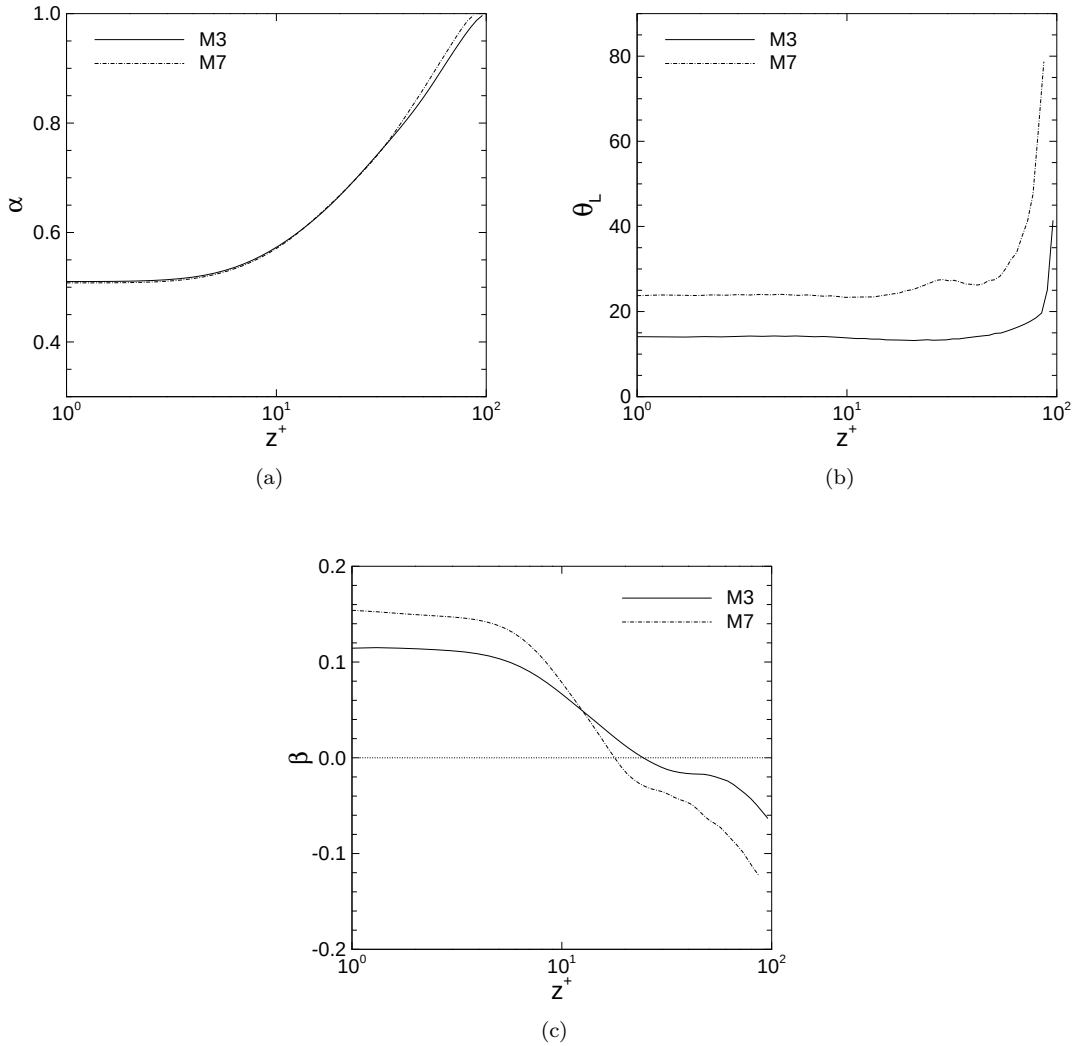

Figure 4. Universal parameters (a) α, (b) θ_L, and (c) β.

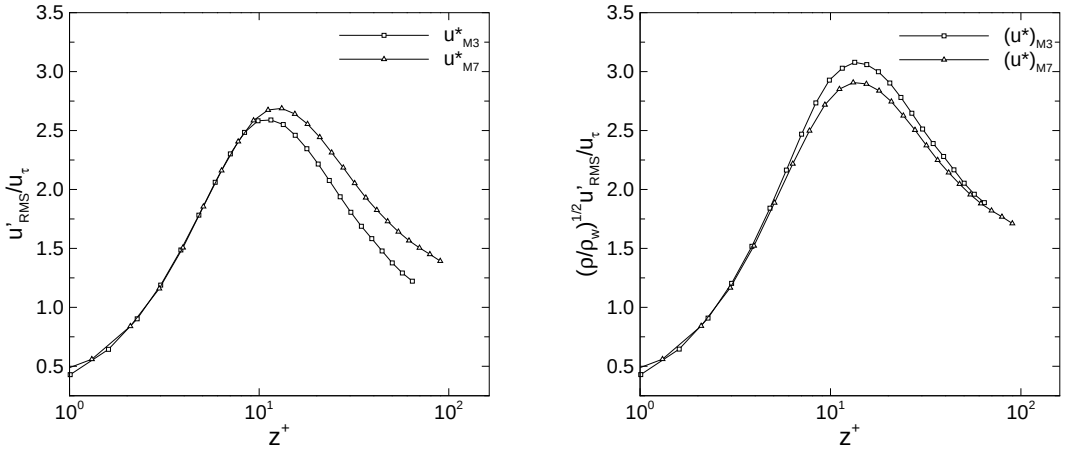

(a) (b)

Figure 5. Universal signal streamwise velocity intensities (a) with no density weighting and (b) with density weighting.

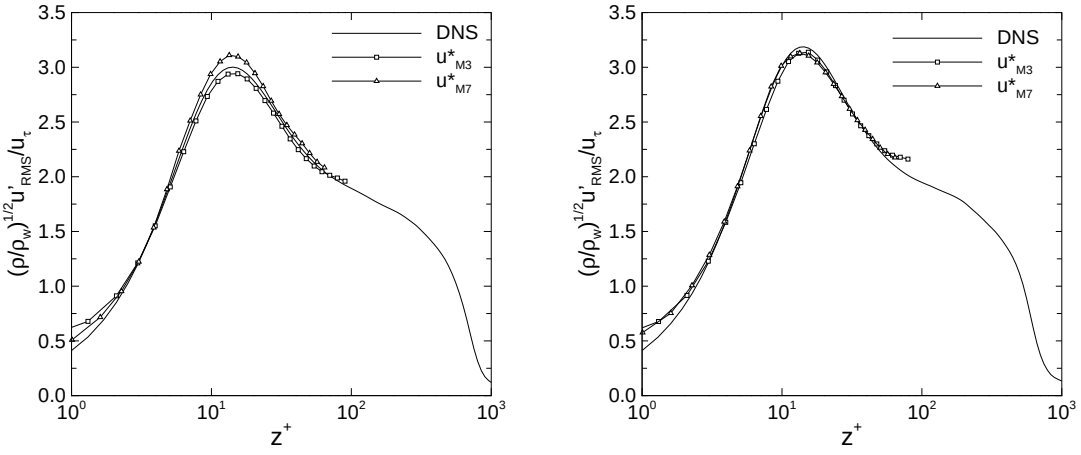

(a) (b)

Figure 6. Density weighted predicted signal streamwise intensities for (a) Mach 3 and (b) Mach 7.

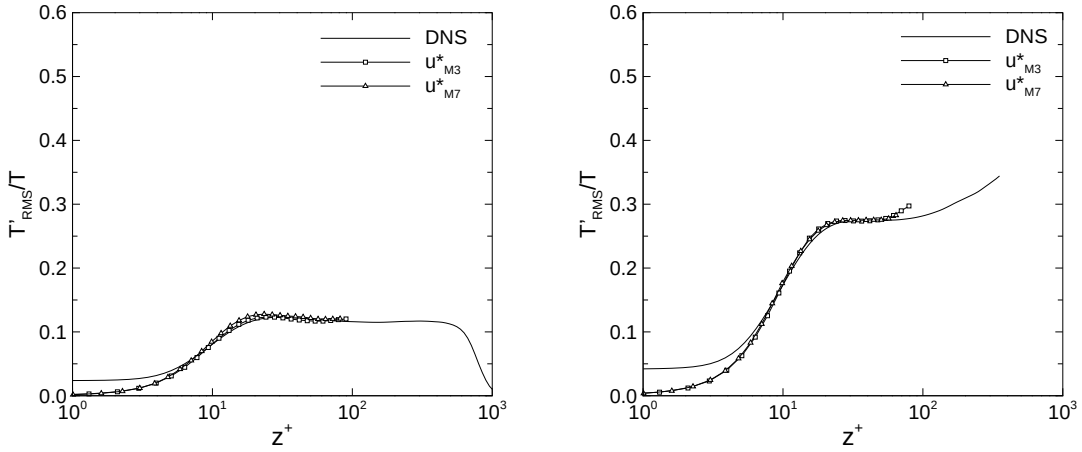

Figure 7. Predicted temperature fluctuation intensities for (a) Mach 3 and (b) Mach 7.

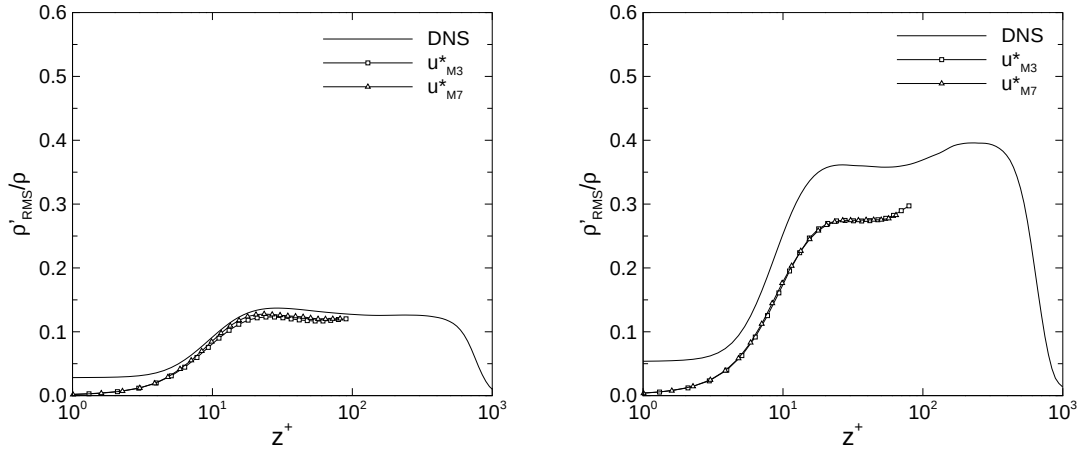

Figure 8. Predicted density fluctuation intensities according to equation 5 for (a) Mach 3 and (b) Mach 7.

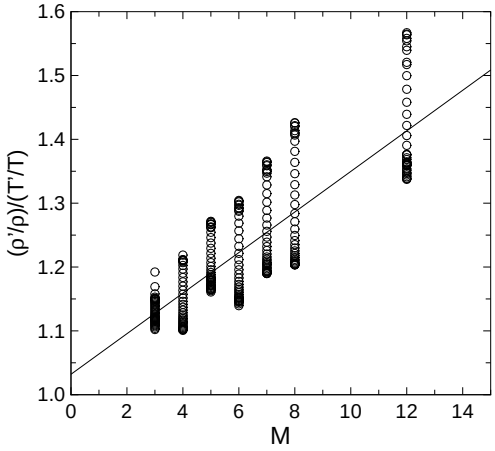

Figure 9. Curve fit to data for the ratio of density to temperature fluctuations versus Mach number.

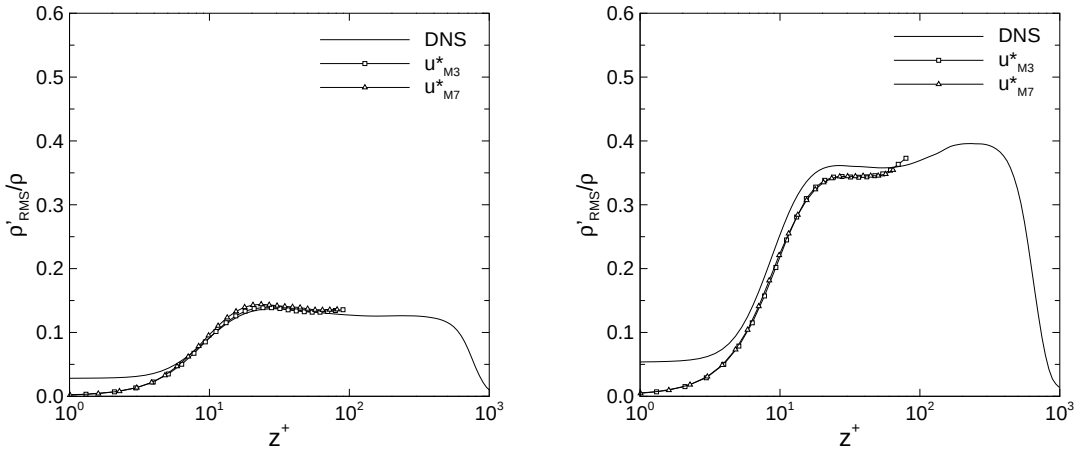

Figure 10. Predicted density fluctuation intensities according to equation 6 for (a) Mach 3 and (b) Mach 7 with Mach number scaling.